Spatial and temporal controls on watershed ecohydrology in the northern Rocky Mountains

Ryan E. Emanuel,[1,2] Howard E. Epstein,[3] Brian L. McGlynn,[4] Daniel L. Welsch,[5] Daniel J. Muth,[3] and Paolo D'Odorico[3]

Received 16 November 2009; revised 26 August 2010; accepted 3 September 2010; published 24 November 2010.

[1] Vegetation water stress plays an important role in the movement of water through the soil-plant-atmosphere continuum. However, the effects of water stress on evapotranspiration (ET) and other hydrological processes at the watershed scale remain poorly understood due in part to spatially and temporally heterogeneous conditions within the watershed, especially in areas of mountainous terrain. We used a spatially distributed model to understand and evaluate the relationship between water stress and ET in a forested mountain watershed during the snow-free growing season. Vegetation water stress increased as the growing season progressed, due to continued drying of soils, and persisted late into the growing season, even as vapor pressure deficit decreased with lower temperatures. As a result, ET became decoupled from vapor pressure deficit and became increasingly dependent on soil moisture later in the growing season, shifting from demand limitation to supply limitation. We found water stress and total growing season ET to be distributed nonuniformly across the watershed due to interactions between topography and vegetation. Areas having tall vegetation and low topographic index experienced the greatest water stress, yet they had some of the highest evapotranspiration rates in the watershed.

Citation: Emanuel, R. E., H. E. Epstein, B. L. McGlynn, D. L. Welsch, D. J. Muth, and P. D'Odorico (2010), Spatial and temporal controls on watershed ecohydrology in the northern Rocky Mountains, *Water Resour. Res.*, *46*, W11553, doi:10.1029/2009WR008890.

1. Introduction

[2] Evapotranspiration is the major flux of water and energy from vegetated land surfaces, and it is closely linked to carbon cycling and vegetation characteristics in terrestrial ecosystems due to the biophysical link between transpiration and CO_2 assimilation [e.g., *Eagleson*, 1982; *Rodriguez-Iturbe and Porporato*, 2004]. Evapotranspiration is also an important sink for soil moisture within the root zone [*Albertson and Kiely*, 2001]. When soil moisture falls below a critical level (whether by ET or other means), vegetation experiences water stress, the result of which is a reduced ability to assimilate atmospheric CO_2 [e.g., *Guswa*, 2005; *Detto et al.*, 2006; *Emanuel et al.*, 2007a]. Since current carbon stores and CO_2 assimilation rates are dictated in part by past rates of CO_2 uptake [*Kozlowski*, 1992], the very structure and organization of a vegetated landscape including both above and belowground vegetation contain information about historical patterns of water stress and ET. Thus, the ability to quantify and understand water stress and its effects on ET within terrestrial ecosystems is important for understanding not only hydrological processes but also the hydrological controls on carbon cycling and on the structure and distribution of vegetation. In areas such as the subalpine forests of the northern Rocky Mountains, understanding how water stress functions and affects carbon and water cycles is very important in light of the climate-driven trend toward earlier snowmelts and reduced snowpacks in this region [e.g., *Fyfe and Flato*, 1999; *Stewart et al.*, 2004; *Mote et al.*, 2005; *Barnett et al.*, 2008].

[3] At larger spatial scales, water stress and ET are dependent on topography and vegetation. Topographic control of soil moisture through patterns of drainage and connectivity [e.g., *Grayson et al.*, 1997; *Mohanty and Skaggs*, 2001] may extend to ET and vegetation water stress through the water-limited processes described above. Vegetation may control ET directly through scaling by leaf area [*Zhang et al.*, 2001] or it may operate on ET indirectly by affecting the aerodynamic properties of canopies [*Anderson et al.*, 2003]. Additionally, vegetation type influences the degree of water stress experienced by plants under a particular set of atmospheric and soil moisture conditions [*Emanuel et al.*, 2007a]. Topography and vegetation thus interact to influence the spatial variability of both water stress and ET, and it is important to characterize (i.e., quantify) the spatial heterogeneity of these processes and their controls to better understand carbon and water cycling at the landscape scale.

[4] For watershed scale studies, ET has traditionally been calculated as the residual unknown in the annual water

[1]Department of Geology, Appalachian State University, Boone, North Carolina, USA.
[2]Now at Department of Forestry and Environmental Resources, North Carolina State University, Raleigh, North Carolina, USA.
[3]Department of Environmental Sciences, University of Virginia, Charlottesville, Virginia, USA.
[4]Department of Land Resources and Environmental Sciences, Montana State University, Bozeman, Montana, USA.
[5]Canaan Valley Institute, Davis, West Virginia, USA.

0043-1397/10/2009WR008890

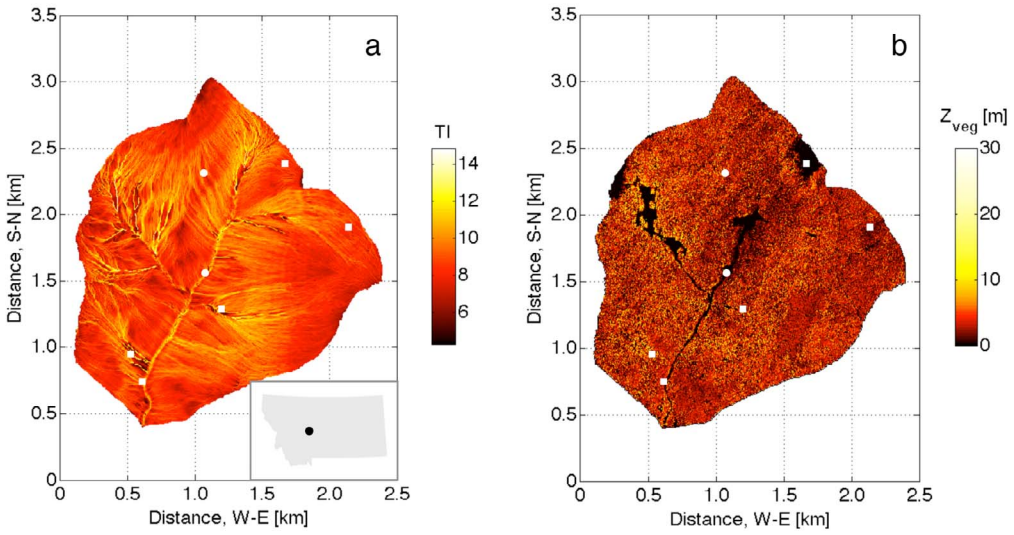

Figure 1. Map of the Stringer Creek watershed showing (a) topographic index TI and (b) distribution of vegetation heights Z_{veg} derived from 1 m ALSM data. White circle shows location of flux tower and white squares show locations of ancillary meteorological stations.

balance [*Dingman*, 2002]. Although useful for low-resolution studies, such estimates of ET are of little help to understanding controls on ET that act at time scales shorter than 1 year or spatial scales smaller than the watershed as a whole. For studies over shorter time scales, flux towers have become a common method for measuring ET directly using techniques such as eddy covariance; however, the areal extent of a tower footprint may or may not represent adequately the heterogeneity of topography and vegetation within a watershed. Even where a flux tower footprint can be assumed to approximate watershed-wide conditions, measurements of ET will reflect average conditions within the footprint, homogenizing the spatial variability caused by differences in topography and vegetation. Although flux towers provide relatively reliable measurements of ET at the landscape scale (typically on the order of 1 km^2 or more for forest ecosystems, depending on vegetation height, surface roughness, and stability of the atmospheric boundary layer), investigations of the spatial and temporal heterogeneity of ecohydrological processes at finer spatial scales within the watershed (approximately 1 m^2 to 1 ha) require estimates of ET at the resolution of topographic and vegetation features within the watershed. Moreover, whereas tree level measurements of transpiration (i.e., sap flux measurements) address the spatial heterogeneity over subwatershed areas, scaling of these measurements to the entire watershed remains difficult [*Ford et al.*, 2007; *Kumagai et al.*, 2008], particularly in the absence of concurrent surface evaporation measurements.

[5] Despite the important role played by ET in land surface hydrology, plant physiology, and climate dynamics, it is unclear how interactions between plant ecophysiology and watershed processes determine the spatial and temporal variability of ET across multiple scales. The purpose of this study is to understand controls on the spatial and temporal variability of ET within a forested watershed. Specifically, we couple a point-based ecohydrological model of vegetation water stress with a spatially distributed hydrological model to provide spatial and temporal descriptions of vegetation water stress within a catchment that allow us to determine (1) what factors contribute to the development of catchment-wide water stress during the growing season in a semiarid, montane forest and (2) what factors cause water stress and ET to evolve and behave differently across a vegetated watershed. By investigating the physical and biological controls on the temporal and spatial heterogeneity of ET during the course of a growing season, we also use this framework to evaluate the impacts of micrometeorology, topography, and vegetation on streamflow.

[6] To investigate these controls we consider as a case study the ecohydrologic dynamics in a subalpine forest of the Rocky Mountains. These forests are important sinks for atmospheric CO_2 in North America [*Schimel et al.*, 2002] and are affected by hydrologic controls, as they lie in semiarid climates, where spring snowmelt provides ecosystems with most of their annual influx of water [*Running*, 1980; *Bales et al.*, 2006]. As a result these forests experience a seasonal decline in soil moisture and, frequently, extended water stress during the growing season. Thus, in these forests CO_2 uptake and ET are closely coupled. This coupling, combined with seasonal patterns of moisture availability as well as mountain topography, make these systems ideal for studying coupled hydrological and ecological processes in a watershed context.

2. Methods

2.1. Site Description and Field Methods

[7] Data were collected during the snow-free portion of the 2006 growing season (22 June through 4 September 2006) within the upper Stringer Creek watershed, a heavily instrumented, 300 ha subcatchment located in the Tenderfoot Creek Experimental Forest (TCEF, Montana, USA; Figure 1). The study site is a forested, subalpine watershed ranging in elevation from 2090 to 2430 m. The watershed is dominated by lodgepole pine (*Pinus contorta*) forest, but it also contains small areas (9% of the watershed) of riparian and upland meadows and isolated areas of subalpine fir (*Abies lasiocarpa*)

and Engelmann spruce (*Picea engelmannii*). In general, however, the watershed has been characterized as even-aged, low-diversity lodgepole forest [*Mincemoyer and Birdsall*, 2006]. The soils are cryoboralfs with a sandy loam texture.

[8] On average, TCEF receives more than 70% of its 880 mm of mean annual precipitation as snow [*McCaughey*, 1996], and it experiences a relatively steady drying of soils throughout the growing season [*Riveros-Iregui et al.*, 2007]. As a result, the temporal dynamics of soil moisture at TCEF are relatively simple; the seasonal dry-down is the dominant trend in soil moisture time series. Soils throughout the watershed transition from relatively wet at the beginning of the growing season to relatively dry at the end. This trend, combined with the relatively simple and uniform ecological structure of the site, makes TCEF well suited for our investigation.

[9] Long-term measurements at this site include snow depth, snow water equivalent, and streamflow [*McCaughey*, 1996; *Woods et al.*, 2006], and since 2005, tower-based measurements of ecosystem fluxes and micrometeorology over the lodgepole forest (measured at 30 m) and separately over a riparian meadow (measured at 1.5 m). Tower-based measurements of interest to this study include ET measured by eddy covariance using a triaxial sonic anemometer (CSAT3, Campbell Scientific, Logan, UT) and open-path infrared gas analyzer (LI7500, Licor Biosciences, Lincoln, NE), air temperature and relative humidity (HMP45C, Campbell Scientific), photosynthetically active radiation (PAR, LI190, Licor Biosciences), net radiation (CNR1, Kipp and Zonen, Delft, Netherlands), and precipitation (tipping buckets, TE525, Texas Electronics, Dallas, TX). Standard tilt correction, spike filtering, sonic anemometer virtual temperature correction, and Webb correction were performed on half-hourly eddy covariance fluxes [*Webb et al.*, 1980; *Schotanus et al.*, 1983; *Kaimal and Finnegan*, 1994; *Paw U et al.*, 2000]. Tower-based micrometeorological measurements were complemented by nests of soil instruments (three per tower) measuring soil temperature at 2.5 and 7.5 cm (Thermocouple, Omega Engineering, Stamford, Conn.), soil heat flux at 5 cm (HFT3, Radiation and Energy Balance Systems, Inc., Seattle, WA), and soil moisture integrated over 0–30 cm using time domain reflectometry (CS616, Campbell Scientific). Separate CS616 probes were also used to measure soil moisture near each tower at 20 cm below ground.

[10] At the beginning of the study period and approximately 3 weeks after snowmelt ended five weather stations (HOBO Micro Station, Onset Computer Corporation, Bourne, MA) were installed in the watershed to provide additional input data for the watershed model. These weather stations measured air temperature and relative humidity at 1 m above the ground surface. Two of the five weather stations measured precipitation using additional tipping buckets. In addition to meteorological data, leaf level ecophysiological data were collected at regular intervals (two to three times per week) from 30 m × 30 m sampling plots surrounding each station using a portable photosynthesis system (LI6400, Licor Biosciences) following the methods of *Norman et al.* [2006]. Leaf chamber measurements (3157 total measurements) collected from the plots were used to estimate parameters for the leaf level ecophysiological model (section 2.3) for two general vegetation types in the watershed, namely conifers and grasses/forbs using nonlinear regression as described by *Emanuel et al.* [2007a]. Leaf chamber measurements were accompanied by shallow (0–20 cm) soil moisture measurements using a handheld TDR probe (HydroSense, Campbell Scientific). Together, these seven stations (two flux towers and five weather stations) cover the major combinations of elevation, aspect, and vegetation type present in the Stringer Creek watershed (Figure 1).

2.2. Remote Sensing of Topography and Vegetation

[11] In September 2005, airborne light detection and ranging (lidar) measurements were collected over approximately 50 km^2 of the TCEF, including the upper Stringer Creek watershed by the National Center for Airborne Laser Mapping (NCALM, Berkeley, CA). First return (canopy top) and last return (bare earth) elevations were recorded as discrete point data and interpolated to 1 m^2 digital elevation models (DEMs) in postprocessing. Two model inputs were derived from the lidar data: a topographic index and an index of vegetation height. The topographic index (*TI*) was calculated from the bare earth DEM (Figure 1a). The digital elevation model was coarsened from 1 to 5 m^2 horizontal resolution using bilinear interpolation, and *TI* was computed as

$$TI = \ln\left(\frac{a}{DI}\right), \tag{1}$$

where a is the specific area contributing to flow through a point in the watershed computed following the algorithm of *Seibert and McGlynn* [2007], and *DI* is the downhill index, an alternative to the local slope that considers topographic concavity downhill of each point by determining how far downhill a parcel of water must travel to lose a certain amount of potential energy [*Hjerdt et al.*, 2004]. In this watershed, the main advantage of *DI* over local slope is the ability to use a high resolution DEM without introducing unrealistic sensitivity of flow to microtopography. Thus, *DI* provides an improved representation of topographic influences on flow in this watershed over the local slope.

[12] In addition to *TI*, an index of vegetation height Z_{veg} was calculated as the difference in elevation between the first and last lidar returns (i.e., the difference between the canopy top elevation and the ground surface elevation), which was coarsened from 1 to 5 m^2 using bilinear interpolation (Figure 1b). Similar lidar-derived vegetation height indices have been shown to accurately represent ground-based measurements of vegetation height [*Dubayah and Drake*, 2000; *Lefsky et al.*, 2002]. Spectral data were not available to discriminate between vegetation types (trees versus grasses/forbs); thus grid cells having $Z_{veg} > 0.5$ m were classified as conifers, and cells having $Z_{veg} \leq 0.5$ m were classified as grasses/forbs. In addition to classification, Z_{veg} was used to derive leaf area index (LAI), a necessary model input, using site-specific allometric relationships given by *Keane et al.* [2005] for lodgepole pine at TCEF. For grass/forb grid cells, we estimated LAI to be 1.0 m^2 m^{-2}. We treated LAI as static through the model simulation period.

2.3. Model Framework

[13] A model of land-atmosphere exchange was developed to simulate coupled hydrological and ecological processes through time as functions of spatially heterogeneous soil, vegetation, and micrometeorological conditions. The model

simulated soil moisture as well as water fluxes from the catchment, including evapotranspiration and runoff.

[14] For the spatially distributed modeling of water fluxes through the soil-plant-atmosphere continuum, we developed and used a spatially extended Soil-Vegetation-Atmosphere-Transfer (SVAT) model. This type of model can provide reliable estimates of ET because it can account for heterogeneity of ET at spatial scales below that of the footprint of flux towers typically used to measure surface water vapor and energy fluxes; however, spatially distributed information about land cover and hydrometeorological conditions is required. This type of model has seen broad use in recent years [e.g. *Famiglietti and Wood*, 1994; *Houser et al.*, 1998; *Boegh et al.*, 2004; *Scanlon et al.*, 2005; *Detto et al.*, 2006]. Detailed SVAT models may scale ET from leaf to landscape scale by applying spatially distributed data to biophysical and energy balance calculations that determine evaporation and transpiration separately. Tower-based measurements of ET may then serve to constrain and validate spatially averaged model estimates. Our SVAT modeling framework includes a TOPMODEL-based subsurface flow and runoff component [*Beven and Kirkby*, 1979] adapted from *Scanlon et al.* [2005] coupled with an ecohydrological model of stomatal conductance. Together, TOPMODEL and the ecohydrological model are used to determine the water balance for each grid cell in the watershed

$$\frac{d\theta}{dt} = \frac{1}{d_{rz}}(I - ET - q_v - q_l), \tag{2}$$

where θ is root zone soil moisture, d_{rz} is the depth of the root zone, I is infiltration, ET is evapotranspiration, q_v is vertical soil water drainage, and q_l is lateral soil water drainage. TOPMODEL estimates groundwater discharge, root zone (unsaturated) discharge, and overland flow based on a conceptual framework of topographic similarity as defined by the topographic index (equation (1)), and these discharges may be combined to simulate total runoff from the watershed [e.g., *Scanlon et al.*, 2005].

[15] The ecohydrological model calculates vegetation stomatal conductance and transpiration based on a framework for modeling the dynamic threshold for water stress presented by *Emanuel et al.* [2007a]. Calculating the dynamic threshold for water stress requires that stomatal conductance be modeled as two separate processes, a soil moisture-independent process where stomatal conductance is a function of the biochemical demand for carbon (i.e., photosynthesis), and a soil moisture-dependent process where stomatal conductance responds to plant hydrodynamics.

[16] We derived a moisture-independent, biochemical model of stomatal conductance by combining a Farquhar-type photosynthesis model [*Farquhar et al.*, 1980; *Collatz et al.*, 1991] with a modified Ball-Woodrow-Berry model of stomatal conductance [*Ball et al.*, 1987; *Leuning*, 1995]. This model assumes similarity among biochemical processes of C_3 plants and is also based on a semiempirical relationship between photosynthetic assimilation rate and stomatal conductance. The resulting model of stomatal conductance does not account for the effect of water stress induced by soil water deficit.

[17] For the hydrodynamic model of stomatal conductance, we selected a steady state model of soil-plant water transfer with four physiological parameters [*Gao et al.*, 2002]. This model considers transpiration as the steady state balance between two diffusion processes: transpiration is expressed as diffusion of water vapor between the water-saturated stomatal cavity and the atmosphere, and soil to leaf water flux is expressed as a laminar flow driven by water potential gradients between the soil and leaf. Leaf water potential is related to stomatal conductance by assuming a linear (elastic) dependence of guard cell deformation on leaf water potential, where osmotic potential is expressed as a semiempirical function of PAR [*Gao et al.*, 2002; *Buckley et al.*, 2003; *Emanuel et al.*, 2007a]. Although this semiempirical relationship between PAR and conductance has been criticized for lack of causality [*Buckley et al.*, 2003], the model is parsimonious compared to other hydrodynamic models of stomatal conductance, which may include 20 or more parameters, and it captures the main factors and processes that determine moisture controls on stomatal function.

[18] Using the framework by *Emanuel et al.* [2007a], stomatal conductance is calculated as the minimum between the values obtained with the moisture-independent biochemical model and with the hydrodynamic model. This approach accounts for limitations arising both from soil water availability and photosynthetic capacity, and for the switching between these two controls. We used model values of stomatal conductance to calculate transpiration, which was, in turn, included in the calculation of soil moisture availability for the next time step. This approach also facilitates calculation of the dynamic threshold of vegetation water stress (ψ_*), which is the soil water potential where switching occurs between biochemical and hydrodynamic stomatal control. The water stress threshold is calculated following *Emanuel et al.* [2007a] as

$$\psi_* = \frac{g_s(1 + k_{\beta g} d_v) - g_{0m} - k_{\alpha\beta} Q}{k_\psi}, \tag{3}$$

where d_v and Q are vapor pressure deficit and PAR, respectively, g_s is biochemically limited stomatal conductance, and the remaining terms ($k_{\beta g}$, g_{0m}, $k_{\alpha\beta}$, and k_ψ) are parameters from a hydrodynamic model of stomatal conductance. The status of vegetation water stress may be determined by comparing ψ_* to actual soil water potential, ψ_s (i.e., vegetation is stressed if ψ_* exceeds ψ_s).

[19] The combined SVAT model simulates volumetric soil water content in the root zone (estimated to be 60 cm deep based on observations from soil pits and from excavations for the flux tower foundation in 2005) by solving the soil water balance equation for every 5 m grid cell at 30 min time steps. Given micrometeorological inputs and initial states of root zone soil water content and catchment discharge (determined from field observations of soil moisture and discharge), the model estimates discharge (groundwater, root zone, and overland flow discharges) and transpiration using the previously described ecological and hydrological modeling frameworks. The model calculates evaporation of canopy and litter interception and litter moisture (from a single, lumped pool at each grid cell) using the direct Priestley-Taylor method [*Priestley and Taylor*, 1972] of determining potential evapotranspiration (PET) and considering evaporation to be the minimum of PET and available water from this pool.

[20] This modeling framework makes a few assumptions and simplifications concerning homogeneity of soil texture, soil thickness, and rooting depth, with important implications for the texture-based relationships between volumetric soil water content and actual soil water potential ψ_s, the calculation of soil moisture dynamics, and water controlled stomatal conductance (hydrodynamic submodel). Moreover, by assuming static ecological structure (e.g., no biomass accumulation, litterfall, nutrient cycling), we ignore seasonal changes as plants allocate carbon to new growth or experience senescence. This assumption is reasonable based on the short length of this study (72 days) relative to the slow growth of lodgepole pines in subalpine ecosystems [see *Ryan and Waring*, 1992]. Finally, ET modeled at any individual point is subject to uncertainty because we assume simple canopy aerodynamics by calculating both the canopy boundary layer resistance and aerodynamic resistance (to water vapor) based on spatial interpolation over complex terrain of wind velocity measurements collected at two points.

[21] Of the model parameters, d_{rz} was estimated by direct observation of soil depths from excavated pits. Other soil parameters, including field capacity and porosity were estimated from the time series of soil moisture measured at the forest flux tower. The TOPMODEL groundwater recession parameter was determined using the recession curve analysis of *Scanlon et al.* [2000], applied to the Stringer Creek hydrograph during the study period. Surface interception storage was approximated based on leaf area index. All of the stomatal conductance model parameters were estimated using nonlinear regression analysis applied to leaf chamber measurements described in section 2.1. Three remaining TOPMODEL parameters (saturated hydraulic conductivity, fraction of root zone discharge lost as vertical drainage, and a soil-specific decay constant for unsaturated hydraulic conductivity) [see *Scanlon et al.*, 2005] were calibrated by minimizing the squared error between observed and modeled stream discharge during the study period.

2.4. Atmospheric Data

[22] We framed this model in a spatially explicit fashion, meaning that all atmospheric, soil, topographic, and vegetation inputs were distributed over the entire watershed at 5 m^2 resolution (for a total of 2.4×10^5 grid cells), and model algorithms were evaluated for each grid cell rather than for bins of similar grid cells. Others [*Famiglietti and Wood*, 1994; *Houser et al.*, 1998] have adopted this approach when considering spatial heterogeneity of multiple environmental factors. Precipitation, air temperature, relative humidity, and horizontal wind speed measurements from the flux towers and weather stations, spanning ranges of elevation, aspect and vegetation cover within the Stringer Creek watershed, were interpolated to a 10 m^2 grid using the Spatial Observation Gridding System (SOGS) [*Jolly et al.*, 2005]. These grid cells were subdivided to match the resolution of the 5 m^2 topographic and vegetation inputs. This interpolation scheme was designed to be independent of the spatial scale of the input data, and it was found to have an absolute uncertainty of less than 2.0°C for temperature and less than 3 mb for atmospheric vapor pressure for continental scale measurements interpolated to a few kilometers [*Jolly et al.*, 2005]. Prior to using the SOGS input variables we verified the accuracy of this interpolation method by removing, individually, each of the two flux towers (forest tower and riparian tower) from the SOGS processing and comparing time series of atmospheric measurements from the removed tower to time series data for the tower's location interpolated from the remaining six weather stations. In each case, we found that SOGS, even when reduced by one input station, was at least as accurate as and typically more accurate than the nearest weather station at reproducing air temperature, relative humidity, and atmospheric vapor pressure deficit at the tower. Precipitation and horizontal wind speed interpolations were not assessed because these input variables were not measured at all seven sites. Additional details of the SOGS verification are found in section 3.1 of this paper.

[23] Photosynthetically active radiation and net radiation were assumed spatially homogeneous at the top of the vegetation canopy; however, we approximated the effects of topography on these variables using a terrain-based hillshading algorithm [*Kumar et al.*, 1997; *Pierce et al.*, 2005] to scale radiation and account for differential topographic shading during morning and afternoon hours. We also used a simplified two big-leaf approximation [*Dai et al.*, 2004] based on lidar-derived vegetation heights to simulate the effects of shading and attenuation of radiation vertically within the canopy.

[24] We also simplified the complex relationships among surface heat fluxes, air temperature, and canopy temperature [*Campbell and Norman*, 1998] after comparing measurements of air temperature to canopy surface skin temperature taken at the forest and meadow flux towers with temperature-corrected infrared thermometers (IRTS-P, Apogee Instruments, Logan, UT). For both sites, regressions between 30 min averages of air and surface temperatures were highly correlated (R^2 = 0.91 for forest, R^2 = 0.82 for meadow), their slopes were statistically indistinguishable from unity ($P < 0.05$), and their intercepts were statistically indistinguishable from 0 ($P < 0.05$). For this reason, we used air temperature to represent average canopy temperature for each half hour of the study period.

[25] We used friction velocity (u_*), derived from turbulence measurements at the 30 m forest flux tower to estimate the canopy boundary layer resistance to water vapor (r_b) following *Hicks et al.* [1987] and *Fuentes et al.* [1994] as

$$r_b = \frac{2}{k u_*} \left(\frac{Sc}{Pr} \right)^{2/3}, \quad (4)$$

where k is the von Kármán number, Sc is the Schmidt number for water vapor in air, and Pr is the Prandtl number. Aerodynamic resistance to water vapor transfer was calculated by applying flux tower-based stability corrections for the logarithmic wind profile to neutrally stable wind profiles computed from interpolated wind velocity data [see *Emanuel et al.*, 2007a].

[26] Key features of this SVAT model include (1) calculation and incorporation of a dynamic threshold for vegetation water stress, (2) use of lidar-derived topographical and vegetation structure information, (3) use of the downstream index in the calculation of *TI*, and (4) spatial interpolation of point-based meteorological variables using SOGS. This modeling strategy makes a number of common assumptions and simplifications, yet assimilates a wide range of spatially distributed environmental data to characterize

Table 1. Assessment of SOGS Interpolation of Meteorological Variables for the Two Flux Tower Sites

	MAE	ε_1' (Baseline: Mean Observation)	ε_1' (Baseline: Other Tower)
		Forest Tower	
T_{air}	3.84°C	0.07 (±0.05)	−0.02 (±0.02)
RH	14.50%	0.02 (±0.07)	0.13 (±0.02)
VPD	4.42 mb	0.13 (±0.05)	0.00 (±0.02)
		Riparian Tower	
T_{air}	1.96°C	0.68 (±0.01)	0.48 (±0.02)
RH	10.30%	0.55 (±0.02)	0.37 (±0.02)
VPD	2.40 mb	0.65 (±0.02)	0.43 (±0.02)

ecological and hydrological responses to environmental controls at high temporal resolution.

3. Assessment of Model Performance

3.1. Assessment Methods

[27] Since no method exists for measuring vegetation water stress directly at the spatial or temporal scales represented by the model, we assessed the validity of the model using outputs that could be measured directly (ET and stream discharge), and we also considered these validation results to represent the model's ability to track vegetation water stress. We validated the model at two time scales using three different approaches, each utilizing independent measures of hydrologic conditions within the watershed. At the 30 min time scale, we compared watershed-averaged ET to eddy covariance measurements of ET above the lodgepole forest. This validation method assumes that the flux footprint of the tower is large enough to represent the variability of ET across the study watershed. A conservative estimate of the upwind extent of the flux footprint of 3 km, based on an instrument height of 30 m and a general southerly wind direction, suggests that, in general, the area contributing to the measured flux contains the study site and similar forested areas and terrain. This method tests the ability of the model to capture the short-term response of vegetation to fluctuations in atmospheric and soil conditions. Also at the 30 min time scale, we compared simulated soil moisture in the root zone (0–60 cm) to actual measurements of root zone soil moisture collected from the moisture probes buried near each flux tower at 20 cm below the surface. For each set of observed O and simulated S variables, we used two measures of model performance. First, the mean absolute error (MAE) was calculated for the time series of length N as

$$\mathrm{MAE} = N^{-1}\sum_{i=1}^{N}|O_i - S_i|, \tag{5}$$

following *Legates and McCabe* [1999]. This measure provides an estimate of model performance in absolute units that have relevance to the system under consideration. Second, a comparative measure of model performance, the adjusted coefficient of efficiency, ε_1' was calculated as

$$\varepsilon_1' = 1 - \frac{\sum_{i=1}^{N}|O_i - S_i|}{\sum_{i=1}^{N}|O_i - \overline{O'}|}, \tag{6}$$

where $\overline{O'}$ may be either the mean of observations or a time trend of observations (which could also be another model simulation) with 95% confidence intervals for the statistic derived from percentile method bootstrapping using 100 realizations [*Legates and McCabe*, 1999]. A value of 0 for ε_1' means that the model performed equally as well (i.e., explained as much variation) as $\overline{O'}$. Positive values of ε_1' indicate improvements over, $\overline{O'}$ and negative values of ε_1' indicate that the model performed worse than $\overline{O'}$. In an application such as this one, comparison of modeled residual to time trend residuals provides a more powerful indicator of model performance than comparison against residuals from the mean observed value. For example, observed discharge decreases almost monotonically through the growing season; substitution of a parametric trend for $\overline{O'}$ in equation (6) yields a more meaningful measure of the model's performance versus that trend rather than versus mean discharge.

[28] As another example, when verifying the accuracy of the SOGS weather interpolation, we compared a time series of observations from the riparian flux tower (O) to a time series at this site based on SOGS interpolation of data from the remaining six sites (S). Table 1 shows mean absolute errors for each tower site and adjusted coefficients of efficiency for each tower site, compared to baselines ($\overline{O'}$) of both the observational mean and a time series of data from the other flux tower. For each variable tested (air temperature, relative humidity, and atmospheric vapor pressure deficit) ε_1' reveals that SOGS interpolation is (1) significantly better at predicting each variable than the mean observed value from each site (with the exception of RH at the forest flux tower, where SOGS was not significantly better than mean observed RH from this site) and (2) at least as accurate as using data from one flux tower to represent another location within the watershed. The SOGS algorithm performed better for the riparian tower than for the forest tower because the riparian tower was surrounded by meteorological stations, whereas the forest tower had no meteorological stations to the north or west to bound the interpolation (Figure 1). These comparisons are based on SOGS interpolation from only six of the meteorological stations; for the full simulation, all seven meteorological stations were used (five HOBO weather stations and two flux towers).

[29] We used MAE and ε_1' to compare model simulations of half-hourly and total stream discharge during the study period to actual stream discharge measured by a U.S. Forest Service stream gage at the watershed outlet. We also compared the model estimate of total ET during the study period to actual ET measured by the forest flux tower. These comparisons assess the ability of the model to represent accurately the seasonal hydrologic balance of the watershed, and they provide an estimate of closure between observations and simulations of the major terms in the catchment water balance.

[30] We expressed vegetation water stress for average watershed conditions and for individual grid cells as a probability that ψ_* would exceed the soil water potential (ψ_s) derived from modeled soil moisture using the *Clapp and Hornberger* [1978] relationship

$$\psi_s = \psi_{Sat}\left(\frac{\theta}{n}\right)^{-b}, \tag{7}$$

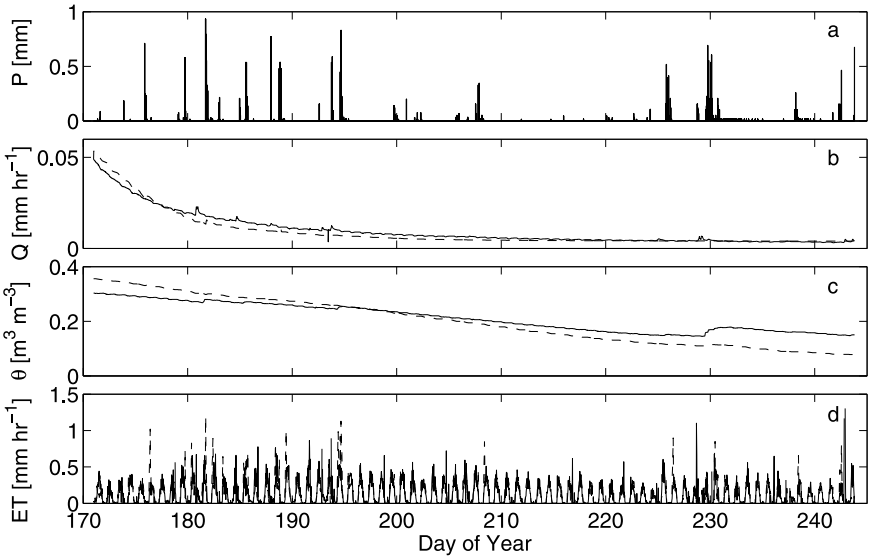

Figure 2. (a) Precipitation observed during the 2006 growing season within the Stringer Creek watershed. (b) Observed (solid line) and modeled (dashed line) stream discharge at the outlet of Stringer Creek. (c) Observed soil moisture at 20 cm depth on a forested hillslope (solid line) and modeled, watershed-average soil moisture θ (dashed line). (d) Observed (solid line) and modeled (dashed line) evapotranspiration within the watershed.

where ψ_{Sat} is the saturation soil water potential, n is porosity, and b is a soil-specific parameter. To account for uncertainty in both the TOPMODEL-derived soil moistures and the conversion from soil moisture to water potential, we used a 500-iteration Monte Carlo simulation to determine a range of likely soil water potential values for average watershed conditions and for each grid cell. For each iteration, the three parameters of equation (7) were selected from uniform distributions based on the range of variability for sandy loam soils documented by *Clapp and Hornberger* [1978]. The probability of water stress for a grid cell during a particular half-hour was calculated as the fraction of the 500 iterations in which ψ_* exceeded ψ_s or $P(\psi_* > \psi_s)$. This value represents the likelihood that water stress occurs at each point in the watershed under present soil and atmospheric conditions, given uncertainty in our estimate of ψ_s. For the analysis of temporal controls on watershed ecohydrology, we considered $P(\psi_* > \psi_s)$ for the average, watershed-wide soil moisture at each time step, $\overline{P(\psi_* > \psi_s)}$. We also computed $P(\psi_* > \psi_s)$ for the 25th and 75th percentiles of soil moisture at time step to determine a realistic range of variability for $\overline{P(\psi_* > \psi_s)}$. For the analysis of spatial controls on watershed ecohydrology, we considered $P(\psi_* > \psi_s)$ for the time-averaged soil moisture conditions at each grid cell in the model, $\langle P(\psi_* > \psi_s)\rangle$. Finally, we evaluated the statistical significance of comparisons between water stress conditions using two-sampled Kolmogorov-Smirnov tests to evaluate differences among cumulative probability distributions and Wilcoxon rank-sum tests to evaluate differences among group medians. Both tests provide P values (P_{KS} and P_W) useful for assessing statistical significance.

3.2. Model Performance and Hydrologic Balance

[31] For the entire time series, ε_1' for modeled ET was 0.44 (±0.04) when compared to a baseline of mean observed ET (Figure 2), meaning that at the half-hourly time scale the model significantly outperformed the mean value of ET. Furthermore, the MAE between observed and simulated half-hourly ET was 0.06 mm h^{-1}, or 1.5 mm d^{-1}. For the entire study period, our SVAT model estimated a total ET loss of 215 mm (46 mm of which was evaporation and 169 mm of which was transpiration), and the forest flux tower measured 213 mm of total ET during the same period. During the 72 day study period, 60 mm of precipitation fell over the study site (Figure 2a), most of which was evaporated from interception storage or litter before infiltrating into the soil. Very little precipitation infiltrated into the root zone relative to the amount of water removed from the root zone by transpiration, which is consistent with earlier findings that snowmelt is the only significant source of soil moisture recharge in subalpine forests of the western United States [*Running*, 1980].

[32] We also compared simulated half-hourly runoff, Q_{sim}, with half-hourly observations of runoff, Q_{obs}, at the watershed outlet and found that the model simulated the observed hydrograph rather well (Figure 2b). For the entire time series, ε_1' for Q_{sim} was 0.69 (±0.02) when compared to the mean of half-hourly Q_{obs}. The MAE between Q_{sim} and Q_{obs} during the study period was 0.002 mm h^{-1} or 0.04 mm d^{-1}. For the entire study period, our SVAT model estimated total runoff to be 16 mm, whereas measured runoff totaled 18 mm. Thus, for the Stringer Creek watershed runoff is an order of magnitude smaller than ET during the growing season. Observations of ET and stream discharge corroborate these model results. Clearly, ET is the dominant watershed scale hydrological flux during the snow-free growing season.

[33] Assessing the validity of simulated soil moisture (Figure 2c) is difficult due to spatial variability inherent in this variable [*Western et al.*, 1999]. We selected two points within the watershed to compare time series of simulated and observed soil moisture. The two points, corresponding to a forested hillslope and a relatively flat riparian meadow,

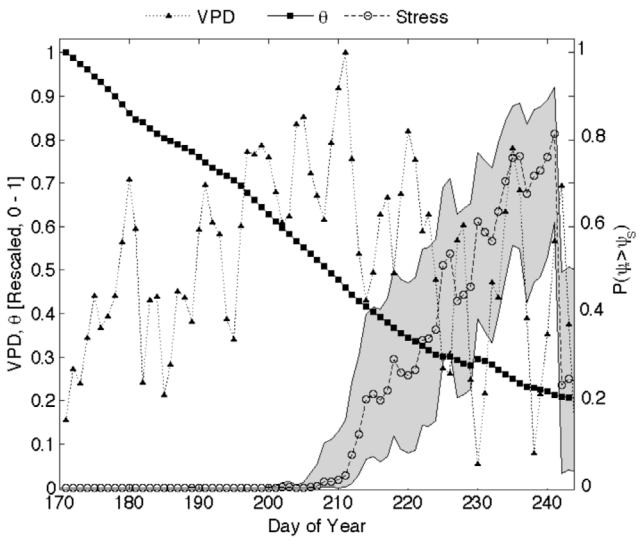

Figure 3. Daytime mean of watershed-averaged probability of water stress $P(\psi_* > \psi_s)$ (open circles) shown with daytime means of vapor pressure deficit (triangles) and volumetric soil moisture (squares). Vapor pressure deficit and volumetric soil moisture have been rescaled from 0 to 1 for plotting on a single axis. Gray area shows range of $P(\psi_* > \psi_s)$ calculated from 25th and 75th percentile of θ at each time step.

were selected for comparison because they represent the two predominant ecosystems within the Stringer Creek watershed. We compared simulated soil moisture θ at the forested grid cell to moisture probe measurements at 20 cm below the surface and found ε_1' to be 0.28 (±0.04) compared to a baseline of mean observed soil moisture at this site and MAE of 0.03 $m^3\ m^{-3}$. Simulated soil moisture at this grid cell declined nearly twice as much (0.28 $m^3\ m^{-3}$) during the study period as observed soil moisture (0.16 $m^3\ m^{-3}$). Despite a low coefficient of efficiency for simulated soil moisture at this forested hillslope location, simulated and measured soil moistures are highly correlated over time ($R^2 = 0.97$).

[34] We also compared simulated θ for a grid cell representing a portion of the riparian meadow to measurements from a moisture probe buried at 20 cm. Here we found, ε_1' to be 0.61 (±0.02) compared to a baseline of mean observed θ at this site, and MAE of 0.03 $m^3\ m^{-3}$. Simulated and measured θ were highly correlated at this site as well ($R^2 = 0.95$). For the meadow site, we also found that the model provided a marginally better estimate of θ than simply using observations of θ from another site (ε_1' was 0.05 ± 0.04 compared to a baseline of soil moisture from the forested hillslope location). In other words, modeled θ was, in general, more realistic than extrapolating forested hillslope θ across the entire watershed.

[35] To understand how well TOPMODEL represented soil moisture dynamics across the watershed in general, we combined shallow soil moisture measurements from five of our seven sampling plots with shallow soil moisture measurements from 53 additional sites collected during the same growing season for a separate study (D. A. Riveros-Iregui, B. L. McGlynn, L. A. Marshall, D. L. Welsch, R. E. Emanuel, and H. E. Epstein, A watershed-scale assessment of a process soil CO_2 production and transport model, submitted to *Water Resources Research*, 2010) to create a data set of shallow soil moisture statistics from 58 sampling sites distributed throughout the upper Stringer Creek watershed. We compared the mean and interquartile range of growing season soil moisture (as a conservative measure of total growing season soil drainage) at each site to lidar-derived TOPMODEL variables a, DI, and TI (equation (1)). We found significant pairwise correlations between mean soil moisture and TI, and mean soil moisture and DI for the data set (Spearman's $\rho = 0.45$, $p < 0.01$ for TI; Spearman's $\rho = 0.47$, $p < 0.01$ for DI). We also found significant pairwise correlations between the interquartile range of soil moisture and both TI and DI (Spearman's $\rho = 0.41$, $p < 0.01$ for TI; Spearman's $\rho = 0.41$, $p < 0.01$ for DI). These results, along with observed correlations between actual and simulated soil moistures at both the forested hillslope and riparian meadow sites, indicate that TOPMODEL characterizes the seasonal dynamics of the soil water balance in this system and the spatial heterogeneity of soil moisture, suggesting that our soil moisture model provides a useful basis for further analysis of spatial and temporal controls on watershed ecohydrology.

4. Results and Discussion

4.1. Temporal Controls on Watershed Ecohydrology

[36] Here we investigate temporal controls on average vegetation water stress conditions within the watershed and provide a context for evaluating controls on average ET within the watershed. The average grid cell within the watershed did not experience water stress, for approximately the first half of the study period (Figure 3). Beginning around day 209 $\overline{P(\psi_* > \psi_s)}$ began to rise, indicating a gradual increase in vegetation water stress throughout the entire watershed. Thus, the growing season may be separated into two regimes: one characterized by a general absence of vegetation water stress within the watershed ($\overline{P(\psi_* > \psi_s)} \approx 0$) and the other characterized by gradually increasing water stress ($\overline{P(\psi_* > \psi_s)} > 0$). The pattern of $\overline{P(\psi_* > \psi_s)}$ in Figure 3 does not mirror that of watershed-averaged θ, suggesting that soil moisture alone does not fully represent and explain the emergence of water stress conditions $\overline{P(\psi_* > \psi_s)}$; rather, some combination of θ and atmospheric controls (represented in Figure 3 by VPD) are acting on vegetation to create a watershed scale stress response manifested as two distinct regimes. Indeed, by definition $\overline{P(\psi_* > \psi_s)}$ is determined both by soil moisture (because of its direct relationship to ψ_s) and by atmospheric controls, which combine with vegetation-specific characteristics to determine ψ_* [*Emanuel et al.* 2007a].

[37] Evaluating differences in hydrologic and atmospheric conditions between the two regimes helps to reveal the processes responsible for determining the status of the watershed with respect to vegetation water stress. Two-sampled Kolmogorov-Smirnov (KS) tests and Wilcoxon rank-sum tests indicate that distributions and median values of modeled ET, θ, VPD, PAR, and air temperature are all significantly different between the unstressed and stressed regimes (Table 2). Differences are reported in standard deviation units for each flux and state variable. The decrease in modeled ET may be considered the response of the watershed to the onset of vegetation water stress, whereas changes in other variables are due to the dependence of ψ_* on soil moisture, light and VPD, and the direct effect of θ on ψ_s. As Figure 3 indi-

Table 2. Comparison of Unstressed Versus Stressed Conditions for the Upper Stringer Creek Watershed[a]

	KS	Δ (σ)	$\rho_{UNSTRESSED}$	$\rho_{STRESSED}$	$\Delta\rho$
ET	0.11	−0.21	–	–	–
θ	0.98	−1.76	−0.03[b]	0.13	0.13
T_{air}	0.10	−0.12	0.75	0.68	−0.07
VPD	0.08	0.11	0.72	0.65	−0.07
PAR	0.06	−0.10	0.92	0.91	−0.01

[a] $P < 0.05$, unless otherwise noted. KS, Kolmogorov-Smirnov statistic; Δ, difference between stressed and unstressed conditions in standard deviation units; ρ, correlation between variable and ET; $\Delta\rho$, difference between stressed and unstressed correlations.
[b] $P = 0.15$.

cates, θ (and thus ψ_s) is most different between stressed and unstressed regimes. However, differences in atmospheric variables are also important when defining these two regimes considering the definition of ψ_* as the soil water potential required to balance the atmospheric demand for water vapor with the rate of CO_2 uptake prescribed by atmospheric conditions [*Emanuel et al.*, 2007a]. Although decreasing air temperature and PAR decrease the capacity for CO_2 uptake by vegetation late in the growing season, continued increases in VPD offset the effect of PAR and air temperature on stomatal conductance and result in an overall rise in ψ_* during the growing season. Continually decreasing ψ_s combined with increasing ψ_* results in an overall increase in $\overline{P(\psi_* > \psi_s)}$ late in the growing season.

[38] Another difference between the unstressed and stressed regimes is the correlation between watershed-average ET and micrometeorological variables (Table 2). The correlation between ET and θ increases from unstressed to stressed conditions within the watershed, whereas the correlation between ET and atmospheric variables (i.e., VPD and T_{air}) decreases from conditions of no water stress to conditions of stress. Thus the transition from unstressed to stressed vegetation is marked by a shift in the functional control of ET from predominantly atmospheric factors and no significant soil moisture control (representing capacity for CO_2 uptake and atmospheric demand for water) to reduced atmospheric control and significant soil moisture control. Not only does the correlation between ET and θ appear at the onset of water stress, but it also strengthens with $\overline{P(\psi_* > \psi_s)}$ (Figure 4), accompanied by a decrease in correlation between ET and atmospheric demand (represented by VPD) decreases (Figure 4). We emphasize here that these correlations are based on observations from the forest flux tower that have been partitioned using modeled levels of catchment-wide water stress.

[39] These patterns of changing correlation suggest that during the growing season, watershed-averaged water stress, and thus watershed-averaged ET are subject to a shift from demand-limitation (controlled by atmospheric variables) to supply limitation (controlled by θ) as the soil water supply decreases relative to the atmospheric demand. As a result ET, which is not limited by θ early in the season, increases with VPD even as θ declines during the unstressed regime. However, once θ is insufficient to meet the atmospheric demand for moisture when stomatal conductance is maximized for CO_2 uptake (a definition of vegetation water stress), ET declines as stomatal conductance is reduced to maintain a sustainable flow of water through the soil-plant-atmosphere continuum. Indeed, watershed-averaged, modeled stomatal

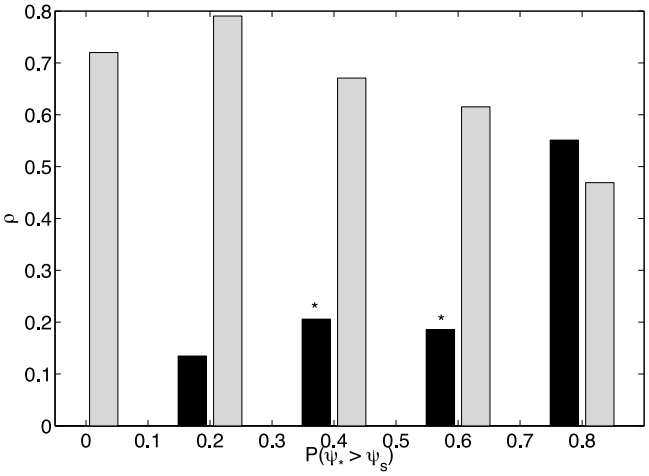

Figure 4. Spearman's coefficient of correlation (ρ) between daytime means of vapor pressure deficit (gray bars) and ET and volumetric soil moisture (black bars) and ET for bins of $P(\psi_* > \psi_s)$. Asterisk indicates no significant difference between levels.

conductance declined by >10% between the unstressed and stressed regimes ($P_W = 0.04$, $P_{KS} < 0.01$). One effect of these shifting controls on the functional relationship between ET and θ is a decrease in ET at both high and low extremes of soil moisture (Figure 5), likely due to low atmospheric demand for moisture (during rainy periods when soil moisture is relatively high [e.g., *Kumagai et al.*, 2004]) or high water stress (during times of low moisture) leading to the pattern of high ET at intermediate soil moisture explained by *Emanuel et al.* [2007b].

4.2. Spatial Controls on Watershed Ecohydrology

[40] Here we use spatially distributed water stress to evaluate the effects of topography and vegetation on spatially distributed ET within the watershed. To do this, we use the *TI*

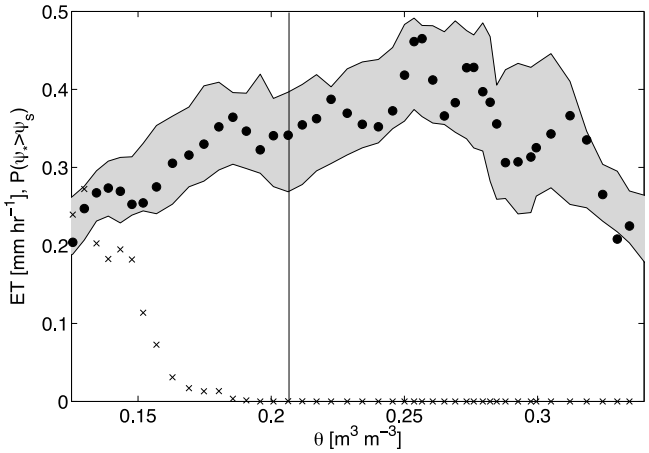

Figure 5. Middday ET (black circles) and daytime range of ET (gray area) as a function of volumetric soil moisture during stressed and unstressed catchment conditions. The vertical line shows the soil moisture level that divides stressed and unstressed conditions, defined as regions where $P(\psi_* > \psi_s) > 0$ (stressed) or $P(\psi_* > \psi_s) = 0$ (unstressed). Midday $P(\psi_* > \psi_s)$ values are shown as black cross marks.

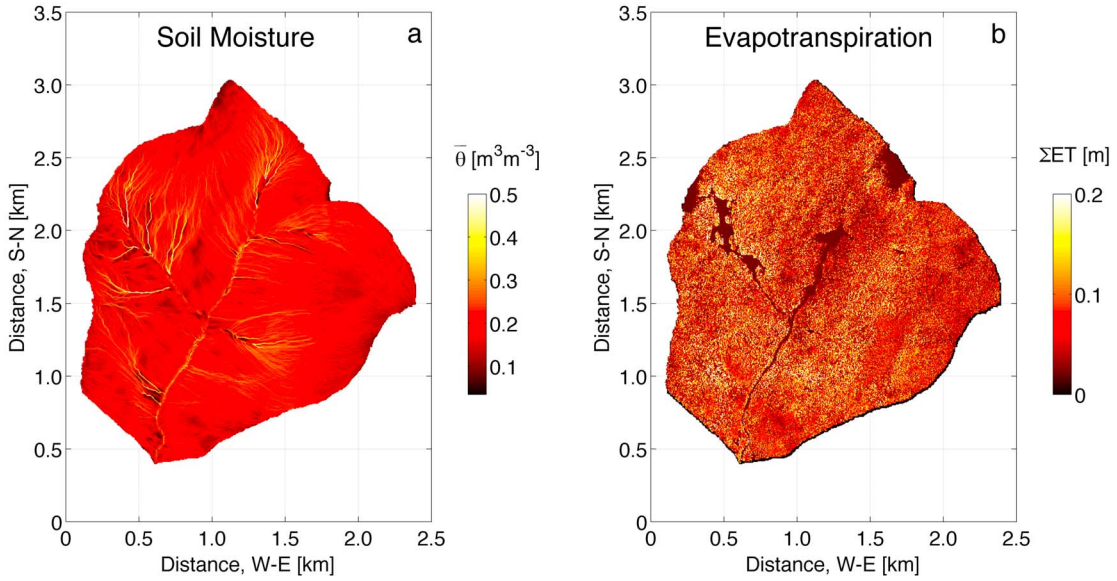

Figure 6. Model simulations of the (a) average soil moisture and (b) total ET distributed throughout the Stringer Creek watershed.

and Z_{veg} as indicators of topography and local vegetation conditions at each 5 m × 5 m grid cell, respectively. Mean growing season soil moisture ($\overline{\theta}$, Figure 6a) and total growing season ET (ΣET, Figure 6b) appear to follow the spatial organization of TI (Figure 1a) and Z_{veg} (Figure 1b), respectively. At first glance, the difference between the spatial organization of these two variables across the watershed suggests that soil moisture does not control ET and that water stress is not a controlling factor. However, despite the high correlation between ΣET and Z_{veg} (due to leaf-to-canopy scaling based on Z_{veg}), many forested grid cells ($Z_{veg} > 0.5$ m) have values of ΣET below the maximum value predicted by Z_{veg}-scaling alone. In fact, the MAE between ΣET and a linear regression model (χ) based solely on Z_{veg} is 51 mm, or approximately 20% of total ET averaged across the watershed. Because the simple model χ considers only tree height and ignores the impact of soil moisture on ΣET, the model's residuals (χ − ΣET) represent, in part, the degree to which soil moisture, and thereby water stress, control ET within the watershed.

[41] By plotting residuals (χ − ΣET) as a function of topography (i.e., TI) and vegetation (i.e., Z_{veg}), the two main sources of spatial heterogeneity within the watershed, areas having low TI and high Z_{veg} emerge as portions of the watershed where ET is controlled by factors other than tree height (Figure 7). These areas, which make up approximately 10% of the watershed and are characterized by relatively tall trees (high Z_{veg}) and relatively dry soils (low TI), have lower evapotranspiration than predicted by χ (i.e., larger residuals). However, this does not mean that these areas necessarily have low ΣET compared to the rest of the watershed. On the contrary, because these areas contain some of the tallest trees and greatest leaf area within the watershed, average ΣET for these grid cells (330 mm) is nearly double the average ΣET for the rest of the watershed (180 mm). If not for water stress, the preceding analysis of residuals suggests that these areas of the watershed would contribute even more to total watershed ET. We evaluate water stress in this portion of Figure 7 (i.e., areas with low χ − ΣET) by considering two spatially distributed metrics, time-averaged probability of water stress and the date of water stress onset. This analysis highlights the importance of considering water stress when using LAI or vegetation height to scale ET between leaf and canopy scales. By scaling modeled ET based on LAI, vegetation height or other structural variables without considering the soil and atmospheric factors contributing to water stress, one runs the risk of overestimating ET. In other words, any univariate relationship between ET and a structural scaling variable should be considered an upper bound to the actual relationship between ET and vegetation structure, made nonlinear by water stress.

[42] The time-averaged probability of vegetation water stress for each grid cell, $\langle P(\psi_* > \psi_s) \rangle$, is correlated primarily with soil moisture or, more precisely, with the sensitivity of modeled $\overline{\theta}$ to TI (Figure 8a, note similarity to Figure 1a). In contrast, the date of water stress onset for each grid cell D_{stress} is correlated primarily with Z_{veg} (Figure 8b, note similarity to Figure 1b). The correlation between D_{stress} and Z_{veg} may result from the tendency of taller trees to have

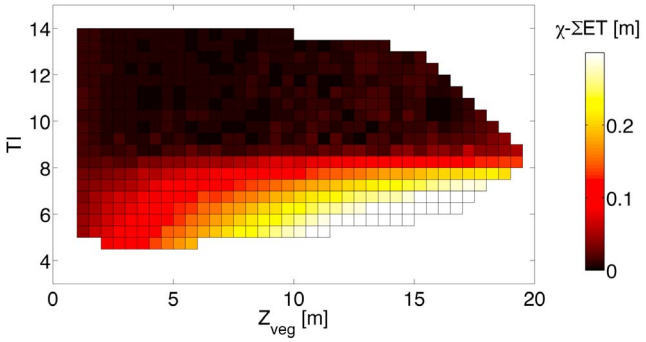

Figure 7. Residuals of linear model χ - ΣET as a function of TI and Z_{veg} for the Stringer Creek watershed.

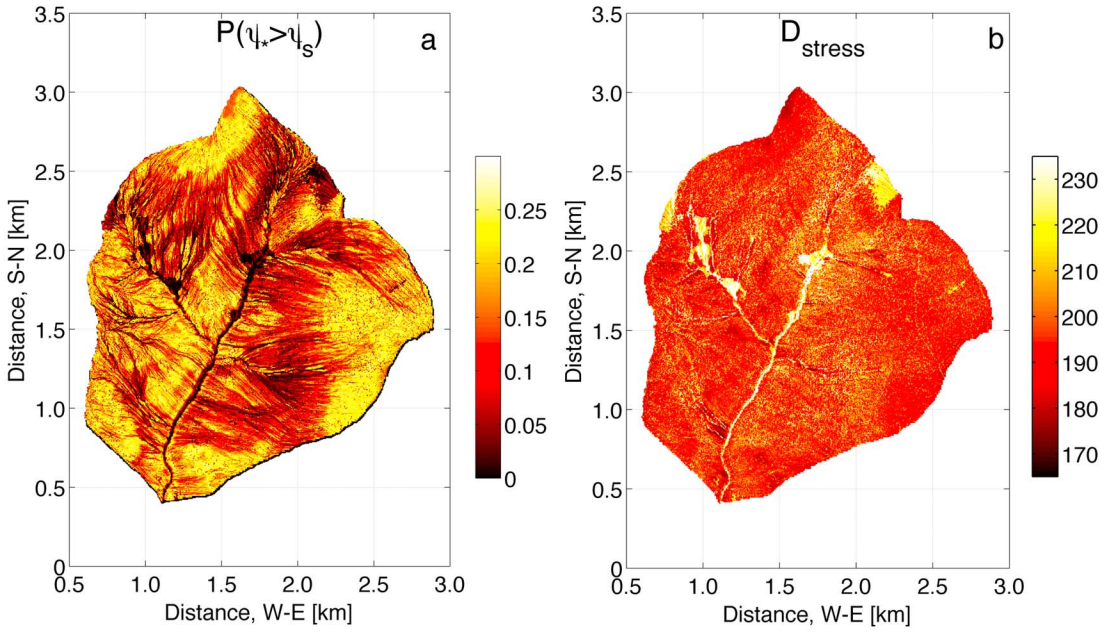

Figure 8. Model simulations of (a) the average probability of water stress during the 2006 growing season and (b) the onset date of water stress for the Stringer Creek watershed.

more leaf area and transpire more water, thus depleting soil moisture earlier in the season.

[43] Both $\langle P(\psi_* > \psi_s)\rangle$ and D_{stress} are useful for interpreting the overall impact of vegetation water stress on ET and other hydrological processes within the watershed, particularly in the low-TI, high-Z_{veg} region defined in Figure 7, because these parts of the watershed contribute, on average, more evapotranspiration than the rest of the watershed (Figure 9a). However, this region experiences significantly higher $\langle P(\psi_* > \psi_s)\rangle$ than the rest of the watershed (Figure 9b). Similarly, this region experiences significantly earlier D_{stress} than the rest of the watershed (Figure 9c). This result confirms that tall trees on relatively dry hillslopes experience more water stress than vegetation in other parts of the watershed, and they also encounter water stress at an earlier date. Increased stress occurs in part because these trees transpire more soil water than other vegetation in the watershed, and also because the hillslopes on which they are located have, on average, only 14% of the uphill contributing area of the rest of the watershed. Thus, small contributing areas combine with tall trees to create water stress, the result of which is to reduce local evapotranspiration in areas of the watershed that already contribute substantially to the water balance of this watershed. These results add to the growing body of evidence for topographic control over vegetation water stress [e.g. *Caylor et al.*, 2005; *Jasper et al.*, 2006] by introducing an ecophysiological basis for modeling spatially distributed water stress and using these model results to interpret flux tower observations.

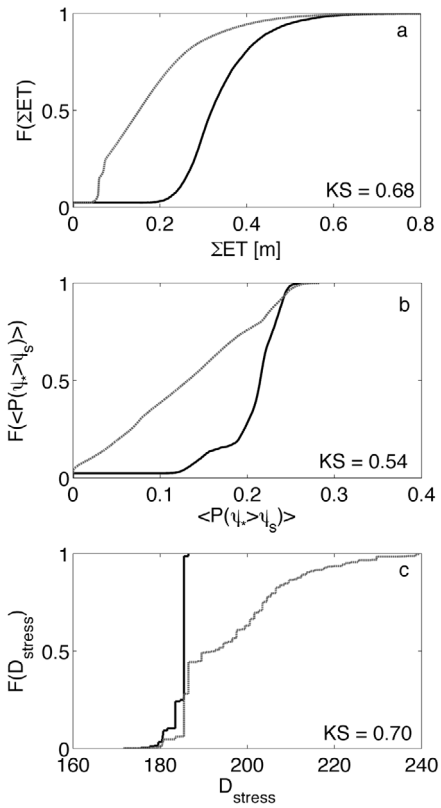

Figure 9. Differences in (a) total ET and (b) average water stress and (c) onset date of water stress for locations where Z_{veg} > 5 m and TI < 8.5 (black line) and for the rest of the watershed (gray line).

4.3. Interaction of Temporal and Spatial Controls

[44] Model results and flux tower measurements indicate that ET is the dominant watershed scale flux during both the unstressed and stressed periods defined in section 4.1,

Table 3. Comparison of Hydrological Fluxes During Unstressed and Stressed Conditions Based on Average Watershed Conditions[a]

Flux	Unstressed (mm d^{-1})	Stressed (mm d^{-1})	Percentage Change
Precipitation	**0.88**	**0.72**	**−18%**
Transpiration	2.58	1.98	−23%[b]
Evaporation	0.72	0.53	−26%
Total ET	**3.31**	**2.51**	**−24%**
Overland q	0.63×10^{-2}	0.01	+60%
Rootzone q	0.23	0.15×10^{-2}	−100%
Groundwater q	9.26×10^{-2}	8.75×10^{-2}	−6%
Total Q_{sim}	**0.33**	**0.10**	**−70%**
$d\theta/dt$	**−2.76**	**−1.89**	**−31%**

[a] $P < 0.05$, unless otherwise noted.
[b] $P = 0.10$.

despite a decline in this flux during the stressed period of the growing season (Table 3). Each of the other hydrological fluxes is reduced significantly during the water-stressed period of the snow-free growing season. However, reduced precipitation alone does not account for the decline in modeled hydrological fluxes between the unstressed and stressed periods. Rather, a combination of reduced precipitation and persistent loss terms (Q_{sim} and ET) cause soil moisture to decline and further affect loss terms that are, themselves, dependent upon soil moisture. Groundwater discharge q_{gw} experiences only a small decline during the study period, but it is a very small component of the hydrological balance compared to other fluxes in Table 3 (with the exception of being the dominant contributor to streamflow during the late growing season). These model results are consistent with recent observations by *Jencso et al.* [2009] that for Stringer Creek, saturated groundwater flow is a small but persistent flux and lateral, root zone flow is highly variable during the growing season.

[45] By volume, ET experiences the greatest absolute seasonal decline, whereas lateral root zone discharge (q_{rz}) experiences the greatest decline on a percentage basis (q_{rz} practically ceases before the end of the growing season.) In fact, q_{rz} declines to 5% of its average unstressed value before day 209, the previously defined transition between unstressed and stressed watershed average conditions. One important aspect of q_{rz} is that, as it nears zero, the lateral redistribution of moisture within the root zone ceases. As a result, soil moisture is no longer replenished by lateral flow from uphill areas of the watershed and is essentially decoupled from topographic control. These two conditions, defined here by the presence or absence of root zone flow, were described by *Grayson et al.* [1997] in terms of nonlocal control (presence of q_{rz}) versus local control (absence of q_{rz}). In terms of this study, nonlocal control of ET is thus characterized by a dependence on TI, and local control of ET is characterized by a dependence on Z_{veg}, where q_{rz} values close to zero mark the transition from nonlocal to local control.

[46] Since the transition from nonlocal to local control of ET within the watershed is determined by q_{rz}, which is a nonlinear function of θ [*Scanlon et al.*, 2005], it follows that this transition is dictated by fluxes that both control θ and are dependent on its state. Evapotranspiration is the largest of these fluxes during the snow-free growing season and therefore the largest sink for θ. Because of this, the transition between nonlocal and local control is driven by spatial controls on ET that remove moisture from the soil (e.g., TI and Z_{veg}) and also by temporal controls on ET such as VPD and θ, both of which act directly on vegetation rather than topography to influence ET. The result of the interaction between spatial and temporal controls in this watershed is a distribution of dates of water stress onset that is primarily correlated with Z_{veg} and, to a much lesser extent, TI (Figure 8b). Thus, an alternate interpretation of D_{stress} is as a map of decoupling dates for atmospheric (demand) or soil moisture (supply) control of ET and also as a map of transition dates from nonlocal (TI) to local (Z_{veg}) control of ET. Thus at the watershed scale, the timing of the transition from demand-limited ET to supply-limited ET (a definition of vegetation water stress) in response to temporally dynamic environmental control is itself governed by temporally static (at our time scale of interest) but spatially heterogeneous landscape characteristics.

5. Conclusions

[47] We present a model of watershed ecohydrology that combines a point-scale land-atmosphere exchange model with a spatially distributed, modified TOPMODEL. The model reproduces observed ET and streamflow, and it provides insight into the temporal and spatial controls on ecohydrological conditions within a northern Rocky Mountain watershed. Specifically, the model simulates both watershed-averaged and spatially distributed vegetation water stress, and it provides a mechanism for explaining observed patterns in the response of ET to environmental controls during the growing season. During the course of the growing season, hydrological controls on ET shift from atmospheric factors to soil moisture as VPD increases and θ decreases. Total ET during the growing season is affected both by TI and Z_{veg} as they interact to influence vegetation water stress, with areas of tall vegetation (and high LAI) and small contributing area seeing the largest decreases in ET. Model results indicate that high LAI and small contributing areas both may lead to shortages in soil moisture and reductions in ET, suggesting that LAI alone should not be used as an indicator of seasonal ET in areas where growing season water stress is likely.

[48] The onset of water stress represents a decoupling of ET from the atmospheric control and a transition from nonlocal control to local control, but for any given location within the watershed, the timing of this decoupling and transition depends on soil moisture status influenced primarily by vegetation height (due to increased transpiration and soil water loss) and secondarily by topography (due to drainage and accumulation of soil moisture within the watershed). Areas having tall vegetation and low topographic index experienced the greatest water stress during the growing season, yet they maintained some of the highest evapotranspiration rates in the watershed. This research investigates the mechanisms by which spatially distributed vegetation has the potential to interact with topographic controls and atmospheric controls on hydrological processes and affect not only ET but soil moisture status and streamflow as well. It also identifies regions of the forested watershed that are both large contributors to the watershed scale ET flux and potentially sensitive to changes in soil moisture availability. In environments such as the northern Rocky Mountains where water stress has the potential to influence vegetation activity and

where ET is a dominant watershed scale flux, the spatial distribution of vegetation is an important characteristic with implications for other watershed scale fluxes.

[49] **Acknowledgments.** This research was funded by NSF grants EAR-0236621, EAR-0403924, and EAR-0838193 and a Moore Research Award from the Department of Environmental Sciences, University of Virginia. We thank W. Matt Jolly (U.S. Forest Service) for providing SOGS code and Todd Scanlon (University of Virginia) for providing TOPMODEL code. We are grateful to the U.S. Forest Service Rocky Mountain Research Station, especially Ward McCaughey, for extensive logistical support. Kelly Caylor (Princeton University), Pat Yeh (University of Tokyo), and an anonymous reviewer provided helpful comments on the manuscript.

References

Albertson, J. D., and G. Kiely (2001), On the structure of soil moisture time series in the context of land surface models, *J. Hydrol.*, *243*(1–2), 101–119.

Anderson, M. C., W. P. Kustas, and J. M. Norman (2003), Upscaling and downscaling—A regional view of the soil-plant-atmosphere continuum, *Agron. J.*, *95*(6), 1408–1423.

Bales, R. C., N. P. Molotch, T. H. Painter, M. D. Dettinger, R. Rice, and J. Dozier (2006), Mountain hydrology of the western United States, *Water Resour. Res.*, *42*, W08432, doi:10.1029/2005WR004387.

Ball, J. T., I. E. Woodrow, and J. A. Berry (1987), A model predicting stomatal conductance and its contribution to the control of photosynthesis under different environmental conditions, *Prog. Photosynth. Res.*, *4*, 221–224.

Barnett, T. P., et al. (2008), Human-induced changes in the hydrology of the western United States, *Science*, *319*, 1080–1083.

Beven, K. J., and M. J. Kirkby (1979), A physically based, variable contributing area model of basin hydrology, *Hydrol. Sci. Bull.*, *24*(1) 43–69.

Boegh, E., M. Thorsen, M. B. Butts, S. Hansen, J. S. Christiansen, P. Abrahamsen, C. B. Hasager, N. O. Jensen, P. Van der Keur, and J. C. Refsgaard (2004), Incorporating remote sensing data in physically based distributed agro-hydrological modelling, *J. Hydrol.*, *287*(1–4), 279–299.

Buckley, T. N., K. A. Mott, and G. D. Farquhar (2003), A hydromechanical and biochemical model of stomatal conductance, *Plant Cell Environ.*, *26*(10), 1767–1785.

Campbell, G. S., and J. M. Norman (1998), *An Introduction to Environmental Biophysics*, 2nd ed., Springer, New York.

Caylor, K. K., S. Manfreda, and I. Rodriguez-Iturbe (2005), On the coupled geomorphological and ecohydrological organization of river basins, *Adv. Water Res.*, *28*, 69–86, doi:10.1016/j.advwatres.2004.08.013.

Clapp, R. B., and G. M. Hornberger (1978), Empirical equations for some soil hydraulic properties, *Water Resour. Res.*, *14*(4) 601–604, doi:10.1029/WR014i004p00601.

Collatz, G. J., J. T. Ball, C. Grivet, and J. A. Berry (1991), Physiological and environmental regulation of stomatal conductance, photosynthesis and transpiration: A model that includes a laminar boundary layer, *Agric. Forest Meteorol.*, *54*(2–4), 107–136.

Dai, Y., R. E. Dickinson, and Y. P. Wang (2004), A two-big-leaf model for canopy temperature, photosynthesis, and stomatal conductance, *J. Clim.*, *17*(12), 2281–2299.

Detto, M., N. Montaldo, J. D. Albertson, M. Mancini, and G. Katul (2006), Soil moisture and vegetation controls on evapotranspiration in a heterogeneous Mediterranean ecosystem on Sardinia, Italy, *Water Resour. Res.*, *42*, W08419, doi:10.1029/2005WR004693.

Dingman, S. L. (2002), *Physical Hydrology*, 2nd ed., 646 p., Prentice Hall, Upper Saddle River, N. J.

Dubayah, R. O., and J. B. Drake (2000), Lidar remote sensing for forestry, *J. For.*, *98*, 44–46.

Eagleson, P. (1982), Ecological optimality in water-limited natural soil-vegetation systems: 1. Theory and hypothesis, *Water Resour. Res.*, *18*(2), 325–340, doi:10.1029/WR018i002p00325.

Emanuel, R. E., P. D'Odorico, and H. E. Epstein (2007a), A dynamic soil water threshold for vegetation water stress derived from stomatal conductance models, *Water Resour. Res.*, *43*, W03431, doi:10.1029/2005WR004831.

Emanuel, R. E., P. D'Odorico, and H. E. Epstein (2007b), Evidence of optimal water use among a range of north american ecosystems, *Geophys. Res. Lett.*, *34*, L07401, doi:10.1029/2006GL028909.

Famiglietti, J. S., and E. F. Wood (1994), Application of multiscale water and energy balance models on a tallgrass prairie, *Water Resour. Res.*, *30*(11), 3079–3094, doi:10.1029/94WR01499.

Farquhar, G. D., S. Von Caemmerer, and J. A. Berry (1980), A biochemical model of photosynthetic CO2 in leaves of C3 species., *Planta*, *149*, 78–90.

Ford, C. R., R. M. Hubbard, B. D. Kloeppel, and J. M. Vose (2007), A comparison of sap flux-based evapotranspiration estimates with catchment-scale water balance, *Agric. Forest Meteorol.*, *145*, 176–185.

Fuentes, J. D., T. J. Gillespie, and N. J. Bunce (1994), Effects of foliage wetness on the dry deposition of ozone onto red maple and poplar leaves, *Water Air Soil Pollut.*, *74*(1–2), 189–210.

Fyfe, L. C., and J. M. Flato (1999), Enhanced climate change and its detection over the Rocky mountains, *J. Clim.*, *12*(1), 230–243.

Gao, Q., P. Zhao, X. Zeng, X. Cai, and W. Shen (2002), A model of stomatal conductance to quantify the relationship between leaf transpiration, microclimate and soil water stress, *Plant Cell Environ.*, *25*(11), 1373–1381.

Grayson, R. B., A. W. Western, F. H. S. Chiew, and G. Bloschl (1997), Preferred states in spatial soil moisture patterns: Local and nonlocal controls, *Water Resour. Res.*, *33*(12), 2897–2908, doi:10.1029/97WR02174.

Guswa, A. J. (2005), Soil-moisture limits on plant uptake: An upscaled relationship for water-limited ecosystems, *Adv. Water Res.*, *28*(6), 543–552.

Hicks, B. B., D. D. Baldocchi, T. Meyers, R. P. Hosker, and D. R. Matt (1987), A preliminary multiple resistance routine for deriving dry deposition velocities from measured quantities, *Water Air Soil Pollut.*, *36*, 311–330.

Hjerdt, K. N., J. J. McDonnell, J. Seibert, and A. Rodhe (2004), A new topographic index to quantify downslope controls on local drainage, *Water Resour. Res.*, *40*, W05602, doi:10.1029/2004WR003130.

Houser, P. R., W. J. Shuttleworth, J. S. Famiglietti, H. V. Gupta, K. H. Syed, and D. C. Goodrich (1998), Integration of soil moisture remote sensing and hydrologic modeling using data assimilation, *Water Resour. Res.*, *34*(12), 3405–3420, doi:10.1029/1998WR900001.

Jasper, K., P. Calanca, and J. Fuhrer (2006) Changes in summertime soil water patterns in complex terrain due to climatic change, *J. Hydrol.*, *327*, 550–563, doi:10.1016/j.jhydrol.2005.11.061.

Jencso, K. G., B. L. McGlynn, M. N. Gooseff, S. M. Wondzell, K. E. Bencala, and L. A. Marshall (2009), Hydrologic connectivity between landscapes and streams: Transferring reach- and plot-scale understanding to the catchment scale, *Water Resour. Res.*, *45*, W04428, doi:10.1029/2008WR007225.

Jolly, W. M., J. M. Graham, A. Michaelis, R. Nemani, and S. W. Running (2005), A flexible, integrated system for generating meteorological surfaces derived from point sources across multiple geographic scales, *Environ. Modell. Software*, *20*(7), 873–882.

Kaimal, J. C., and J. J. Finnegan (1994) *Atmospheric Boundary Layer Flows*, 289 pp., Oxford Univ. Press, New York.

Keane, R. E., E. D. Reinhardt, J. Scott, K. Gray, and J. Reardon (2005), Estimating forest canopy bulk density using six indirect methods, *Can. J. For. Res.*, *35*(3), 724–739.

Kozlowski, T. T. (1992), Carbohydrate sources and sinks in woody plants, *Bot. Rev.*, *82*(2), 107–222.

Kumagai, T., G. G. Katul, T. M. Saitoh, Y. Sato, O. J. Manfroi, T. Morooka, T. Ichie, K. Kuraji, M. Suzuki, and A. Porporato (2004), Water cycling in a Bornean tropical rain forest under current and projected precipitation scenarios, *Water Resour. Res.*, *40*, W01104, doi:10.1029/2003WR002226.

Kumagai, T., M. Tateishi, T. Shimizu, and K. Otsuki (2008), Transpiration and canopy conductance at two slope positions in a Japanese cedar forest watershed, *Agric. For. Meteorol.*, *148*, 1444–1455.

Kumar, L., A. K. Skidmore, and E. Knowles (1997), Modelling topographic variation in solar radiation in a GIS environment, *Int. J. Geogr. Info. Sci.*, *11*(5), 475–497.

Lefsky, M. A., W. B. Cohen, G. G. Parker, and D. J. Harding (2002), Lidar remote sensing for ecosystem studies, *Bioscience*, *52*(1), 19–30.

Legates, D. R., and G. J. McCabe (1999), Evaluating the use of "goodness-of-fit" measures in hydrologic and hydroclimatic model validation, *Water Resour. Res.*, *35*(1), 233–241, doi:10.1029/1998WR900018.

Leuning, R. (1995), A critical appraisal of a combined stomatal-photosynthesis model for C3 plants, *Plant Cell Environ.*, *18*(4), 339–355.

McCaughey, W. W. (1996), Tenderfoot creek experimental forest, in *Experimental Forests, Ranges, and Watersheds in the Northern Rocky Mountains: A Compendium of Outdoor Laboratories in Utah, Idaho, and Montana*, edited by W. C. Schmidt and J. L. Friede, U.S. Dep. of Agriculture, Forest Service, Utah.

Mincemoyer, S. A., and J. L. Birdsall (2006), Vascular flora of the Tenderfoot Creek Experimental Forest, Little Belt Mountains, Montana, *Madroño*, *53*(3), 211–222.

Mohanty, B. P., and T. H. Skaggs (2001), Spatio-temporal evolution and time-stable characteristics of soil moisture within remote sensing foot-

prints with varying soil, slope, and vegetation, *Adv. Water Res.*, *24*(9–10), 1051–1067.

Mote, P. W., A. F. Hamlet, M. P. Clark, and D. P. Lettenmaier (2005), Declining mountain snowpack in western North America, *Bull. Am. Meteorol. Soc*, *86*(1), 39–49.

Norman, J. M., J. M. Welles, and D. K. McDermitt (2006), Estimating canopy light-use and transpiration efficiencies from leaf measurements, *Appl. Note 105*, LI-COR Biosci., Lincoln, Nebr.

Paw U., K. T., D. D. Baldocchi, T. P. Meyers, and K. B. Wilson (2000), "Correction of eddy-covariance measurements incorporating both advective effects and density fluxes," *Boundary Layer Meteorol.*, *97*, 487–511.

Pierce, K. B., T. Lookingbill, and D. Urban (2005), A simple method for estimating potential relative radiation (PRR) for landscape-scale vegetation analysis, *Landscape Ecol.*, *20*(2), 137–147.

Priestley, C. H. B., and R. J. Taylor (1972), On the assessment of surface heat flux and evaporation using large-scale parameters, *Mon. Weather Rev.*, *100*, 81–92.

Riveros-Iregui, D. A., R. E. Emanuel, D. J. Muth, B. L. McGlynn, H. E. Epstein, D. L. Welsch, V. J. Pacific, and J. M. Wraith (2007), Diurnal hysteresis between soil temperature and soil CO_2 is controlled by soil water content, *Geophys. Res. Lett.*, *34*, L17404, doi:10.1029/2007GL030938.

Rodriguez-Iturbe, I., and A. Porporato (2004), *Ecohydrology of Water-Controlled Ecosystems*, 442 pp., Cambridge Univ. Press, New York.

Running, S. W. (1980), Relating plant capacitance to the water relations of pinus contorta, *For. Ecol. Manage.*, *2*(4), 237–252.

Ryan, M. G., and R. H. Waring (1992), Maintenance respiration and stand development in a subalpine lodgepole pine forest, *Ecology*, *73*(6), 2100–2108.

Scanlon, T. M., J. P. Raffensperger, G. M. Hornberger, and R. B. Clapp (2000), Shallow subsurface stormflow in a forested headwater catchment: Observations and modeling using a modified TOPMODEL, *Water Resour. Res.*, *36*(9) 2575–2586, doi:10.1029/2000WR900125.

Scanlon, T. M., G. Kiely, and R. Amboldi (2005), Model determination of nonpoint source phosphorus transport pathways in a fertilized grassland catchment, *Hydrol. Processes*, *19*(14), 2801–2814.

Schimel, D., T. G. F. Kittel, S. Running, R. Monson, A. Turnispeed, and D. Anderson (2002), Carbon sequestration studied in western U.S. mountains, *Eos Trans. AGU*, *83*(40), 445–449, doi:10.1029/2002EO000314.

Schotanus, P., F. T. M. Nieuwstadt, and H. A. R. De Bruin (1983), Temperature measurement with a sonic anemometer and its application to heat and moisture fluxes, *Boundary Layer Meteorol.*, *26*, 81–93.

Seibert, J., and B. L. McGlynn (2007), A new triangular multiple flow direction algorithm for computing upslope areas from gridded digital elevation models, *Water Resour. Res.*, *43*, W04501, doi:10.1029/2006WR005128.

Stewart, I. T., D. R. Cayan, and M. D. Dettinger (2004), Changes in snowmelt runoff timing in western North America under a 'business as usual' climate change scenario, *Clim. Change*, *62*(1–3), 217–232.

Webb, I. K., G. I. Pearman, and R. Leuning (1980), Correction of flux measurements for density effects due to heat and water vapour transfer, *Q. J. R. Meteorol. Soc.*, *106*, 85–100.

Western, A. W., R. B. Grayson, G. Bloschl, G. R. Wilgoose, and T. A. McMahon (1999), Observed spatial organization of soil moisture and its relation to terrain indices, *Water Resour. Res.*, *35*(3), 797–810, doi:10.1029/1998WR900065.

Woods, S. W., R. Ahl, J. Sappington, and W. McCaughey (2006), Snow accumulation in thinned lodgepole pine stands, Montana, USA, *Forest Ecol. Manage.*, *235*(1–3), 202–211.

Zhang, L., W. R. Dawes, and G. R. Walker (2001), Response of mean annual evapotranspiration to vegetation changes at catchment scale, *Water Resour. Res.*, *37*(3), 701–708, doi:10.1029/2000WR900325.

R. E. Emanuel, Department of Forestry and Environmental Resources, North Carolina State University, PO Box 8008, Raleigh, NC 27695, USA. (ryan_emanuel@ncsu.edu)

P. D'Odorico, H. E. Epstein, and D. J. Muth, Department of Environmental Sciences, University of Virginia, 291 McCormick Rd, Charlottesville, VA 22904, USA.

B. L. McGlynn, Department of Land Resources and Environmental Sciences, Montana State University, Bozeman, MT 59716, USA.

D. L. Welsch, Canaan Valley Institute, Davis, WV 26260, USA.